JCI insight

Cystathionine γ-lyase exacerbates *Helicobacter pylori* immunopathogenesis by promoting macrophage metabolic remodeling and activation

Yvonne L. Latour, Johanna C. Sierra, Jordan L. Finley, Mohammad Asim, Daniel P. Barry, Margaret M. Allaman, Thaddeus M. Smith, Kara M. McNamara, Paula B. Luis, Claus Schneider, Justin Jacobse, Jeremy A. Goettel, M. Wade Calcutt, Kristie L. Rose, Kevin L. Schey, Ginger L. Milne, Alberto G. Delgado, M. Blanca Piazuelo, Bindu D. Paul, Solomon H. Snyder, Alain P. Gobert, Keith T. Wilson

JCI Insight. 2022;7(12):e155338. https://doi.org/10.1172/jci.insight.155338.

Research Article | Gastroenterology | Immunology

Graphical abstract

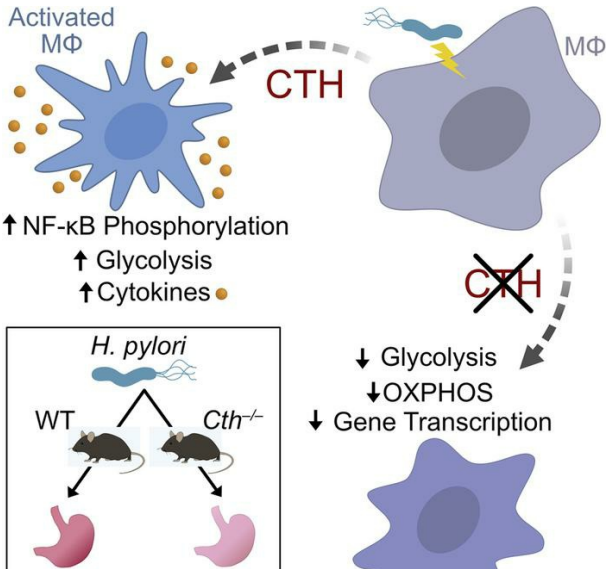

JCI insight

RESEARCH ARTICLE

Cystathionine γ-lyase exacerbates *Helicobacter pylori* immunopathogenesis by promoting macrophage metabolic remodeling and activation

Yvonne L. Latour,[1,2] Johanna C. Sierra,[2,3] Jordan L. Finley,[2] Mohammad Asim,[2] Daniel P. Barry,[2] Margaret M. Allaman,[2] Thaddeus M. Smith,[2] Kara M. McNamara,[2,4] Paula B. Luis,[5] Claus Schneider,[3,5] Justin Jacobse,[1,2] Jeremy A. Goettel,[1,2,3] M. Wade Calcutt,[6] Kristie L. Rose,[6] Kevin L. Schey,[6] Ginger L. Milne,[7] Alberto G. Delgado,[2] M. Blanca Piazuelo,[2,3] Bindu D. Paul,[8,9] Solomon H. Snyder,[8,9,10] Alain P. Gobert,[2,3] and Keith T. Wilson[1,2,3,4,11]

[1]Department of Pathology, Microbiology, and Immunology, [2]Division of Gastroenterology, Hepatology, and Nutrition, Department of Medicine, and [3]Center for Mucosal Inflammation and Cancer, Vanderbilt University Medical Center, Nashville, Tennessee, USA. [4]Program in Cancer Biology, [5]Department of Pharmacology, and [6]Department of Biochemistry, Mass Spectrometry Research Center, Vanderbilt University School of Medicine, Nashville, Tennessee, USA. [7]Division of Clinical Pharmacology, Department of Medicine, Vanderbilt University Medical Center, Nashville, Tennessee, USA. [8]Department of Psychiatry and Behavioral Sciences, [9]Department of Pharmacology and Molecular Sciences, and [10]The Solomon H. Snyder Department of Neuroscience, Johns Hopkins University School of Medicine, Baltimore, Maryland, USA. [11]Veterans Affairs Tennessee Valley Healthcare System, Nashville, Tennessee, USA.

Macrophages play a crucial role in the inflammatory response to the human stomach pathogen *Helicobacter pylori*, which infects half of the world's population and causes gastric cancer. Recent studies have highlighted the importance of macrophage immunometabolism in their activation state and function. We have demonstrated that the cysteine-producing enzyme cystathionine γ-lyase (CTH) is upregulated in humans and mice with *H. pylori* infection. Here, we show that induction of CTH in macrophages by *H. pylori* promoted persistent inflammation. *Cth*$^{-/-}$ mice had reduced macrophage and T cell activation in *H. pylori*–infected tissues, an altered metabolome, and decreased enrichment of immune-associated gene networks, culminating in decreased *H. pylori*–induced gastritis. CTH is downstream of the proposed antiinflammatory molecule, *S*-adenosylmethionine (SAM). Whereas *Cth*$^{-/-}$ mice exhibited gastric SAM accumulation, WT mice treated with SAM did not display protection against *H. pylori*–induced inflammation. Instead, we demonstrated that *Cth*-deficient macrophages exhibited alterations in the proteome, decreased NF-κB activation, diminished expression of macrophage activation markers, and impaired oxidative phosphorylation and glycolysis. Thus, through altering cellular respiration, CTH is a key enhancer of macrophage activation, contributing to a pathogenic inflammatory response that is the universal precursor for the development of *H. pylori*–induced gastric disease.

Conflict of interest: KTW serves as an associate editor for the journal *Gastroenterology*. He receives compensation for this work from the American Gastroenterological Association.

Submitted: September 28, 2021
Accepted: May 10, 2022
Published: June 22, 2022

Reference information: *JCI Insight*. 2022;7(12):e155338. https://doi.org/10.1172/jci.insight.155338.

Introduction

Monocyte-derived macrophages are a key component of the innate immune response, providing a wide range of functions, including response to pathogens, antigen presentation, immune regulation, and wound repair (1–3). In response to bacterial pathogens such as *Helicobacter pylori*, macrophages exhibit an M1-like phenotype that is characterized by expression of genes encoding chemokines and cytokines that orchestrate the recruitment and activation of other innate cells as well as a robust adaptive T cell response that perpetuates inflammation (4–10). Proinflammatory macrophages also express enzymes that produce effector molecules such as NO and ROS, which help limit the pathophysiology of infection (8, 9, 11–13). However, these events can contribute to dysregulation of cellular homeostasis and tissue damage. A unique feature of macrophage biology is the ability to maintain plasticity to regulate the proinflammatory response and/or repair damage in responding to environmental cues and metabolic remodeling (14).

Therefore, understanding the molecular mechanisms that dictate and regulate macrophage activation has therapeutic potential that is still largely unexplored.

Cystathionine γ-lyase (CTH; also known as CSE) breaks down cystathionine into cysteine, α-ketobutyrate, and ammonia as the last step of the mammalian reverse transsulfuration pathway (RTP) (15, 16). Cystathionine is generated by cystathionine β-synthase (CBS) from homocysteine and serine (15). Homocysteine is directly downstream of the demethylation of *S*-adenosylmethionine (SAM) to *S*-adenosylhomocysteine, an important step in DNA, histone, and protein methylation (Figure 1) (17). Another major role of SAM, a product of methionine metabolism, is the biosynthesis of the polyamines spermidine and spermine by spermidine synthase and spermine synthase, respectively (18). Both enzymes require the decarboxylated form of SAM (dcSAM), which is synthesized by the enzyme *S*-adenosylmethionine decarboxylase (SAMDC), to donate an amino-propyl group (Figure 1) (18).

H. pylori is a Gram-negative bacterium that is estimated to colonize approximately 4.4 billion people, making it 1 of the most common bacterial pathogens in humans (19). *H. pylori* is the strongest risk factor for development of gastric adenocarcinoma, the fourth leading cause of cancer mortality in the most recent 2020 GLOBOCAN data (20), with 89% of all gastric cancer cases associated with evidence of *H. pylori* colonization (21, 22). Although complex regimens of antibiotic treatment are available, the prevalence of antibiotic-resistant strains is on the rise (23–25). In addition, the benefit of *H. pylori* eradication in cancer prevention relies on low rates of reinfection and sustained negative *H. pylori* colonization status (26, 27). These issues are compounded by the lack of clinical and biological markers to predict patients at risk for precancerous lesions (28). *H. pylori* elicits a vigorous, yet generally ineffective, innate and adaptive mucosal immune response, resulting in a chronically active inflammatory state that contributes to the progression from gastritis to adenocarcinoma (29–32). Thus, new strategies are needed to target the host immune response to reduce antibiotic use and circumvent the risk of antibiotic resistance.

We recently reported that *H. pylori* upregulates expression of CTH in mouse and human gastric macrophages (Gmacs) and reduces spermidine and spermine synthesis by limiting SAM availability in macrophages in vitro (33). We now present evidence that genetic deletion of *Cth* results in reduced gastritis, suppression of both innate and adaptive immune markers, and downregulation of metabolic pathways, including those involved in cellular respiration with *H. pylori* or with classical macrophage stimuli. These findings were independent of changes in polyamine metabolism. Additionally, there were changes in adaptive immune responses in the gastric mucosa with *Cth* deletion, but effects on T cells appeared to be independent of any effects of CTH within T cells. Taken together, our data suggest that modulation of CTH activity affects the innate immune response of macrophages and pathogenic gastric inflammation, thus representing a potential target for therapeutic intervention in *H. pylori* pathogenesis.

Results

Deletion of Cth reduces gastritis in acute models of H. pylori pathogenesis. We determined that CTH expression was localized to Gmacs in *H. pylori*–infected human stomach tissues and persists at an increased level during progression along the histological cascade toward carcinogenesis (33). Thus, we used *Cth*-deficient mice (34) to determine the role of CTH in vivo during *H. pylori* infection. First, we confirmed that *Cth* mRNA expression is eliminated in the gastric tissues of $Cth^{-/-}$ mice with and without *H. pylori* infection (Figure 2A). Immunofluorescence of infected gastric tissues from WT mice showed colocalization of CTH with $CD68^+$ Gmacs (Figure 2B); deletion of *Cth* led to loss of *H. pylori*–stimulated CTH protein in $CD68^+$ Gmacs (Figure 2B). Then, to assess the effect of CTH in vivo, we used well-established models of *H. pylori* infection: C57BL/6 WT and $Cth^{-/-}$ mice were infected with *H. pylori* strain PMSS1 for 4 or 8 weeks (12, 35). Animals lacking *Cth* demonstrated significantly decreased histologic gastritis at 4 weeks (Supplemental Figure 1, A and B; supplemental material available online with this article; https://doi.org/10.1172/jci.insight.155338DS1) and 8 weeks (Figure 2, C and D), and no difference in histology in uninfected mice (Supplemental Figure 1A). Consistent with our previous studies in other mutant mice (11, 12, 36, 37), decreased levels of gastritis were associated with increased levels of gastric colonization by *H. pylori* in $Cth^{-/-}$ mice (Figure 2, E and F, and Supplemental Figure 1C). Expression of the genes encoding for (a) the proinflammatory marker TNF-α, (b) the antiinflammatory marker arginase 1 (ARGI1), and (c) the Th1 cytokine IFN-γ, were all significantly downregulated in $Cth^{-/-}$ mice infected with *H. pylori* PMSS1 for 4 weeks when compared with infected WT mice (Supplemental Figure 1, D and E).

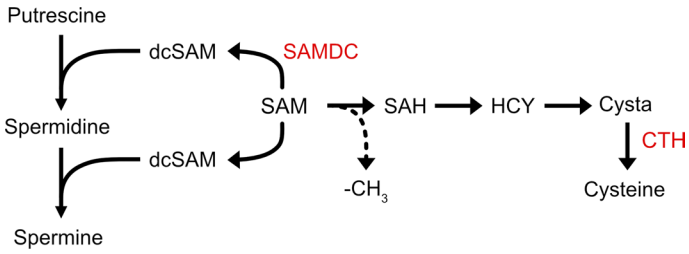

Figure 1. SAM metabolism. Schematic of key metabolites and enzymes (red) downstream of SAM. cysta, cystathionine; HCY, homocysteine; SAH, *S*-adenosyl-L-homocysteine.

CTH mediates induction of immune response–specific gene sets. Because *H. pylori* infection produces a chronic inflammatory state in humans, we used an established mouse model of chronic *H. pylori* infection to assess differential gene expression, in which mice were infected with *H. pylori* strain SS1 for 16 weeks (11, 12). Similar to the acute *H. pylori* infection models, *Cth*$^{-/-}$ mice exhibited significantly decreased histologic gastritis (Figure 3, A and B) and increased *H. pylori* colonization (Figure 3C). Furthermore, the expression of the genes encoding for the proinflammatory genes TNF-α, chemokine (C-X-C motif) ligand 1 (CXCL1; the murine homolog of the neutrophil chemokine IL-8), IL-12β, and for the Th17 marker IL-17 and the Th1 marker IFN-γ were downregulated in *Cth*$^{-/-}$ mice chronically infected with *H. pylori* SS1 for 16 weeks compared with infected WT animals (Figure 3D). Similarly, the transcript of the antiinflammatory marker *Il10* was also higher in WT mice versus *Cth*$^{-/-}$ mice during *H. pylori* infection (Figure 3E). CTH expression was not induced in the Ly6G^{+} neutrophils (Supplemental Figure 2) or CD3^{+} lymphocytes (Supplemental Figure 3A) found in the gastric tissues of infected WT mice. Although WT CD4^{+} splenocytes express increased levels of *Cth* mRNA with costimulation of CD3 and CD28 (Supplemental Figure 3B), *Cth*$^{-/-}$ splenocytes did not exhibit differences in cytokine or T cell transcription factor expression or proliferation compared with WT splenocytes (Supplemental Figure 3, C–E). Thus, CTH is not upregulated in either gastric neutrophils or T cells with *H. pylori* infection, and CTH does not have a primary effect on T cell function. However, our data demonstrate that CTH expression contributes to the gastric immune response to *H. pylori* and affects the macrophage innate response and, hence, the adaptive T cell response.

To evaluate global changes in the transcriptome of Gmacs, we isolated F4/80^{+} cells (Supplemental Figure 4A) from the gastric tissues of WT and *Cth*$^{-/-}$ mice infected with *H. pylori* SS1 for 16 weeks and performed RNA-Seq. Hierarchical clustering and heatmap analysis highlighted differential transcript abundance between genotype and infection status (Supplemental Figure 4B). Principal component analysis demonstrated a distinct distribution of transcript profiles from WT and *Cth*$^{-/-}$ Gmacs that was dependent on *H. pylori* infection (Supplemental Figure 4C). Overall, there were 24,781 transcripts identified that were present in 2 or more samples. Of the total transcripts, 17,246 were known mRNAs and 7535 were unknown. Using a FDR of 0.1, we identified differentially expressed genes (DEGs), downregulated and upregulated, between Gmacs from infected *Cth*$^{-/-}$ and WT mice (Figure 4A). The complete list of DEGs, including Ensemble transcript identifiers, official gene symbols, fold changes, and *P* values, is provided in Supplemental Data Set 1. Gene ontology–term gene set enrichment analysis of the significant DEGs between Gmacs from infected *Cth*$^{-/-}$ versus WT mice evidenced suppression of gene sets associated with immunity and response to stimuli (Figure 4B and Supplemental Data Set 2). Notably, gene-level expression analysis of the gene ontology term "immune system process" revealed consistently reduced expression in Gmacs from infected *Cth*$^{-/-}$ mice compared with WT mice (Figure 4, C and D).

We next determined how the response to infection differs between WT and *Cth*-deficient mice when compared with their respective uninfected controls. We performed differential gene expression analysis to compare the response to infection between genotypes. There were 37 downregulated genes shared by WT and *Cth*$^{-/-}$ Gmacs and 145 genes that were induced in both WT and *Cth*$^{-/-}$ cells during infection (Supplemental Figure 5A). Immune-related genes upregulated by infection in WT Gmacs included *Irgm1*, *Irgm2*, *Ifit1*, and *Ido1*, in addition to upregulated *Cth* expression (Figure 5A). In contrast, immune-related genes were either not induced or were downregulated by infection, such as *Ifit2*, *Cybb*, and *Fcna*, in *Cth*$^{-/-}$ Gmacs (Figure 5B). Pathway analysis of significant DEGs using the Database for Annotation,

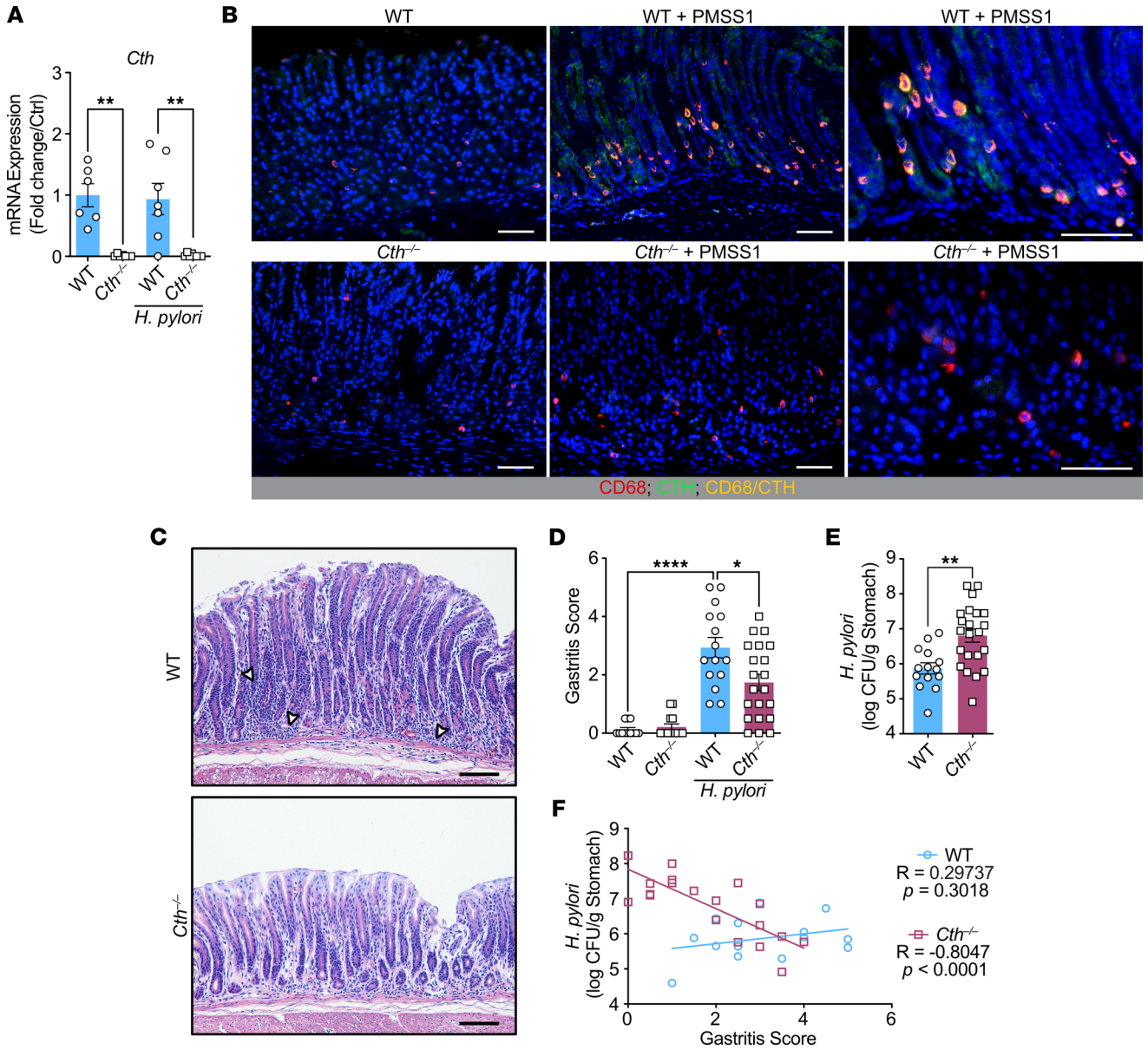

Figure 2. Deletion of *Cth* reduces gastritis in an acute model of *H. pylori* pathogenesis. WT and *Cth*$^{-/-}$ mice were infected or not with *H. pylori* PMSS1 for 8 weeks. (**A**) CTH mRNA expression in gastric tissues of WT and *Cth*$^{-/-}$ mice infected or not with *H. pylori*; *n* = 3–7 mice per genotype. (**B**) Representative immunofluorescence images of CTH (green) colocalized (yellow) with the macrophage marker CD68 (red) from WT and *Cth*$^{-/-}$ mice infected or not with *H. pylori*; *n* = 3 mice per genotype. DAPI (blue). (**C**) H&E images from infected mice; arrowheads highlight inflammatory cells. (**D**) Histologic gastritis scores. Each symbol is a different mouse; data are pooled from 2 independent experiments. (**E**) *H. pylori* colonization in gastric tissues from **D**. (**F**) Correlation between gastritis in **D** and *H. pylori* colonization in **E**. All values are reported as mean ± SEM. Statistical analyses, where shown, are: (**A** and **D**) 1-way ANOVA with Kruskal-Wallis test, followed by a Mann-Whitney *U* test; (**E**) Student's *t* test; (**F**) correlation and significance determined by Pearson's product-moment correlation test. **P* < 0.05, ***P* < 0.01, *****P* < 0.0001. (**B** and **C**) Scale bars: 50 μm. Ctrl, control.

Visualization, and Integrated Discovery Bioinformatics Resource (https://david.ncifcrf.gov/) revealed 4 downregulated pathways from the Kyoto Encyclopedia of Genes and Genome Pathways database in the transcriptome of *Cth*$^{-/-}$ mice compared with WT mice (Supplemental Figure 5B and Supplemental Data Set 3). We also assessed function-associated keywords and identified 26 downregulated keywords (Supplemental Figure 5C). Downregulated pathways and keywords in cells from infected *Cth*$^{-/-}$ mice compared with WT mice included metabolic pathways and the following downregulated keywords: "immunity," "*S*-adenosyl-L-methionine," and "methyltransferase" (Figure 5C and Supplemental Figure 5, B and C). Downregulation of these pathways suggests that Gmacs from *Cth*$^{-/-}$ mice have altered immune function and impaired metabolic activation compared with WT mice. Furthermore, the downregulation

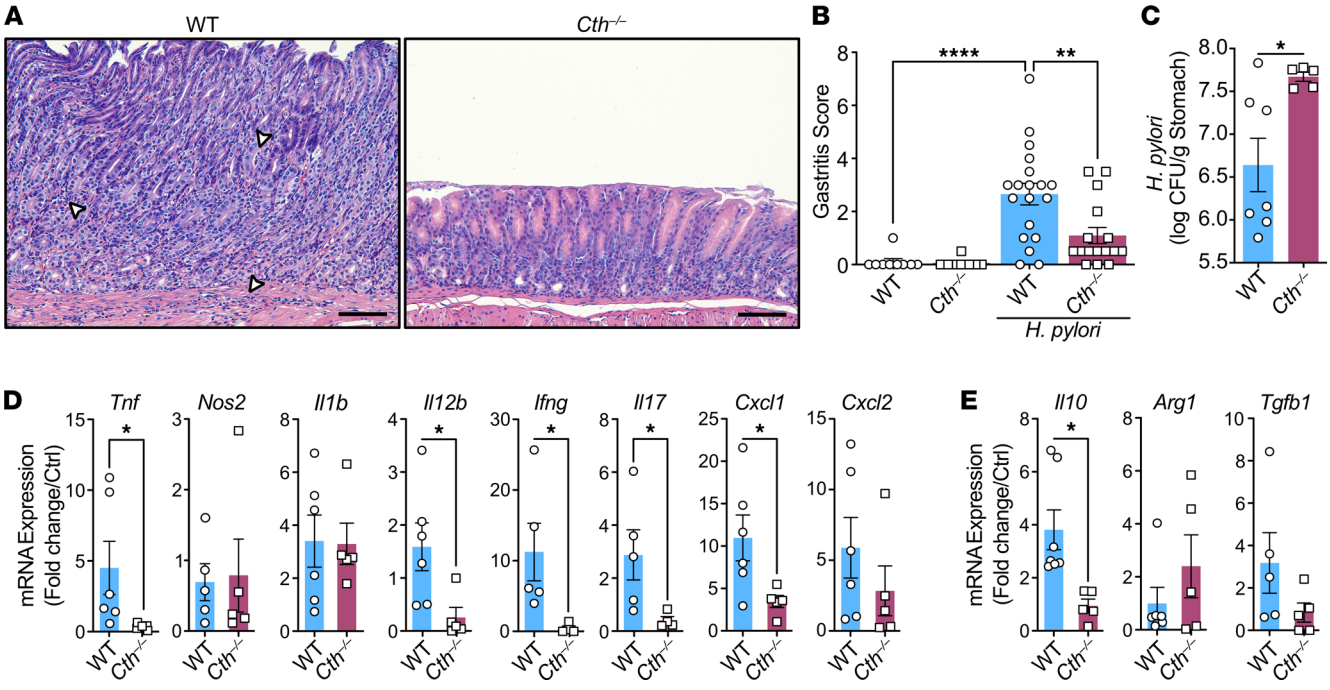

Figure 3. Deletion of *Cth* reduces gastritis in a chronic model of *H. pylori* pathogenesis. WT and *Cth*$^{-/-}$ mice were infected or not with *H. pylori* SS1 for 16 weeks. (**A**) H&E images from infected mice; arrowheads highlight inflammatory cells. (**B**) Histologic gastritis scores. Each symbol is a different mouse; data pooled from 2 independent experiments. (**C**) *H. pylori* colonization in gastric tissues from **B**. (Tissues from 1 of the experiments was used for RNA-Seq). mRNA expression of (**D**) proinflammatory and (**E**) antiinflammatory markers in gastric tissues; n = 5–6 *H. pylori*–infected mice per genotype. (**B–E**) All values are reported as mean ± SEM. Statistical analyses, where shown: (**B**, **D**, and **E**) 1-way ANOVA with Kruskal-Wallis test, followed by a Mann-Whitney U test; (**C**) Student's t test. *$P < 0.05$. (**A**) Scale bars: 50 μm. Ctrl, control.

of genes associated with SAM and methyltransferases is consistent with our hypothesis that CTH activity can modulate the reactions upstream of the RTP.

CTH promotes the metabolism of SAM through the RTP during H. pylori infection. To relate the transcriptional changes to metabolic signatures, we next performed an untargeted global metabolomic analysis of the gastric tissues from infected WT and *Cth*$^{-/-}$ mice. Overall, there were 1300 positively charged metabolites and 734 negatively charged metabolites significantly affected by CTH in infected mice (Supplemental Figure 6, A and B). Pathway analysis evidenced metabolic pathways involving SAM metabolism; namely "(*S*)-reticuline biosynthesis," "spermidine biosynthesis," "spermine biosynthesis," and "L-serine degradation" were significantly affected by deletion of *Cth* in infected mice (Figure 6A and Supplemental Data Set 4). We also found that pathways involved in energy production, such as the TCA cycle and glycolysis, were affected by the deletion of *Cth* (Figure 6A).

We then used targeted metabolomics to verify our findings. Specifically, dcSAM, SAM, and cystathionine levels were measured by liquid chromatography–mass spectrometry in the tissues of WT and *Cth*$^{-/-}$ mice infected or not with *H. pylori* (Figure 6B). Levels of dcSAM remained relatively similar; however, SAM levels were significantly accumulated in naive *Cth*$^{-/-}$ mice and significantly decreased in *Cth*$^{-/-}$ mice with infection with no change in SAM levels in the WT mice (Figure 6B). Importantly, levels of cystathionine, the substrate for CTH, were markedly increased in the *Cth*$^{-/-}$ mice, confirming that CTH activity was lost (Figure 6B).

Because there was an abundance of SAM in naive *Cth*$^{-/-}$ gastric tissues, we investigated whether SAM availability directly regulates the macrophage response to *H. pylori*. We treated bone marrow–derived macrophages (BMmacs) with SAM in the absence or presence of *H. pylori* for 24 hours. We confirmed that exogenous SAM treatment results in accumulation of SAM and cystathionine in the BMmacs, which decreased with infection (Supplemental Figure 7A). Analysis of mRNA expression revealed that treatment with SAM significantly reduced expression of *Tnf* and *Il12b*, while increasing expression of *Il1b* and *Il6*, having no effect on *Nos2* and the p35 subunit of IL-12 (*Il12a*), and increasing expression of the prototypical markers of antiinflammatory macrophages, *Arg1*, and *Tgfb1* (Supplemental Figure 7, B–E). To assess the in

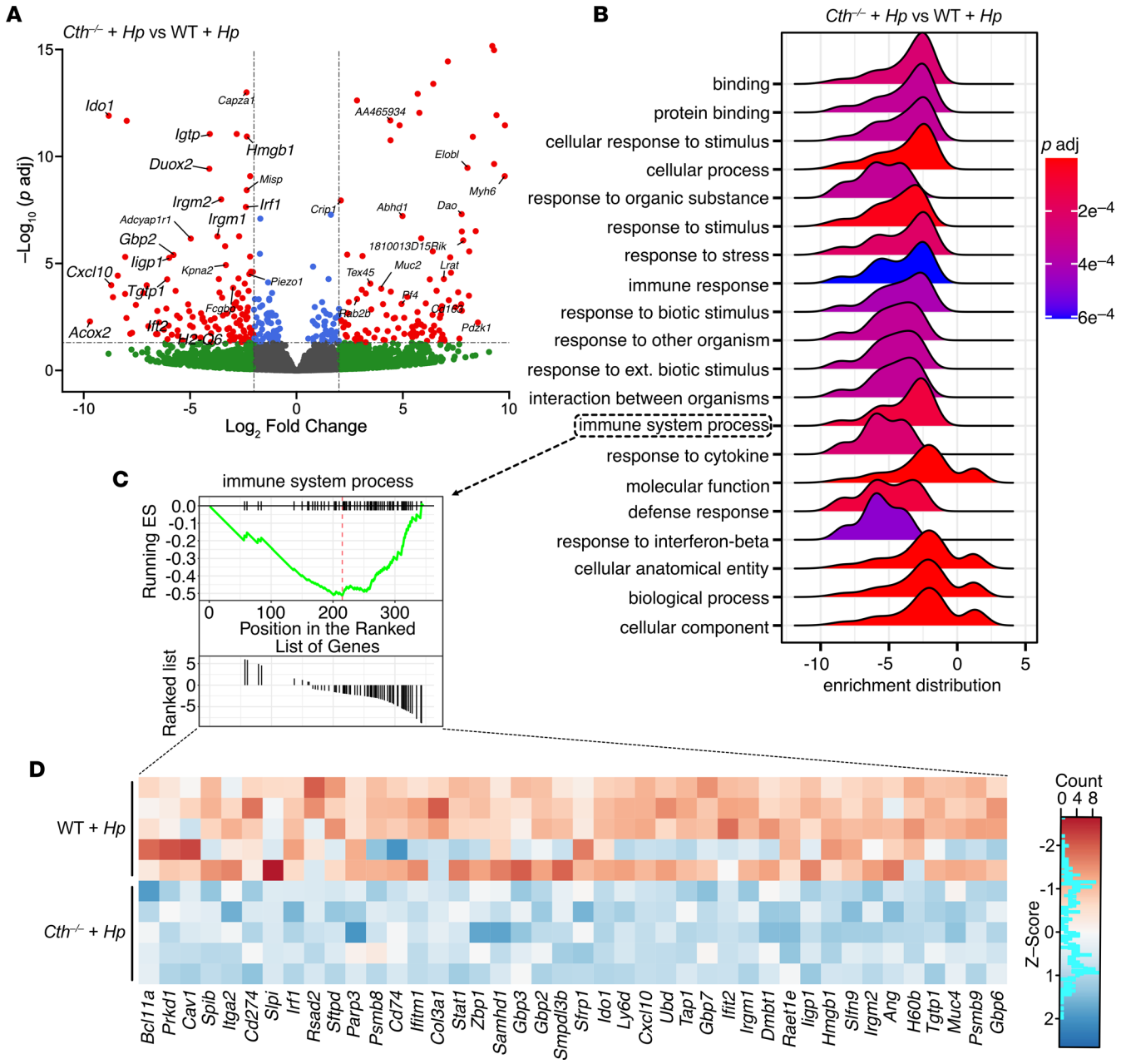

Figure 4. CTH mediates induction of immune response–specific gene sets. Transcriptomic analysis using RNA-Seq of F4/80$^+$ enriched gastric cells (Gmacs); n = 5 individual infected mice per genotype. (**A**) Volcano plot of DEGs in *Cth*$^{-/-}$ Gmacs compared with WT Gmacs from infected mice (fold change [FC] > 2; FDR < 0.05). Immune-associated genes are enlarged. Gray dots, not significant; green dots, $\log_2$ fold change > 2; blue dots, adjusted (adj) P < 0.05; red dots, $\log_2$ fold change > 2 and adjusted (adj) P < 0.05. (**B**) Ridge plot displaying gene set enrichment analysis of DEGs in infected *Cth*$^{-/-}$ compared with infected WT Gmacs ($\log_2$ fold change > 2; FDR < 0.05). (**C**) Enrichment score plot of the gene set "immune system process" identified in **A**. (**D**) Heatmap showing the gene-level expression of genes within the immune system process gene set shown in **B**. Ext, external; ES, ES, enrichment score.

vivo effect of SAM on *H. pylori*–induced disease, WT mice were orally gavaged with SAM starting 1 week after infection (p.i.) (Supplemental Figure 7F). There was no change in gastritis score or colonization after SAM treatment (Supplemental Figure 7, G and H).

CTH is downstream of SAM, which is needed for the biosynthesis of dcSAM, and thus for spermidine and spermine production. We have previously shown that polyamines can regulate *H. pylori*–induced macrophage activation and thus affect disease progression (6, 7, 9, 12, 36). To determine if CTH may affect *H. pylori*–induced immune activation by a mechanism linked to polyamines, we next measured polyamine levels in the gastric tissues of WT and *Cth*$^{-/-}$ mice infected or not with *H. pylori*.

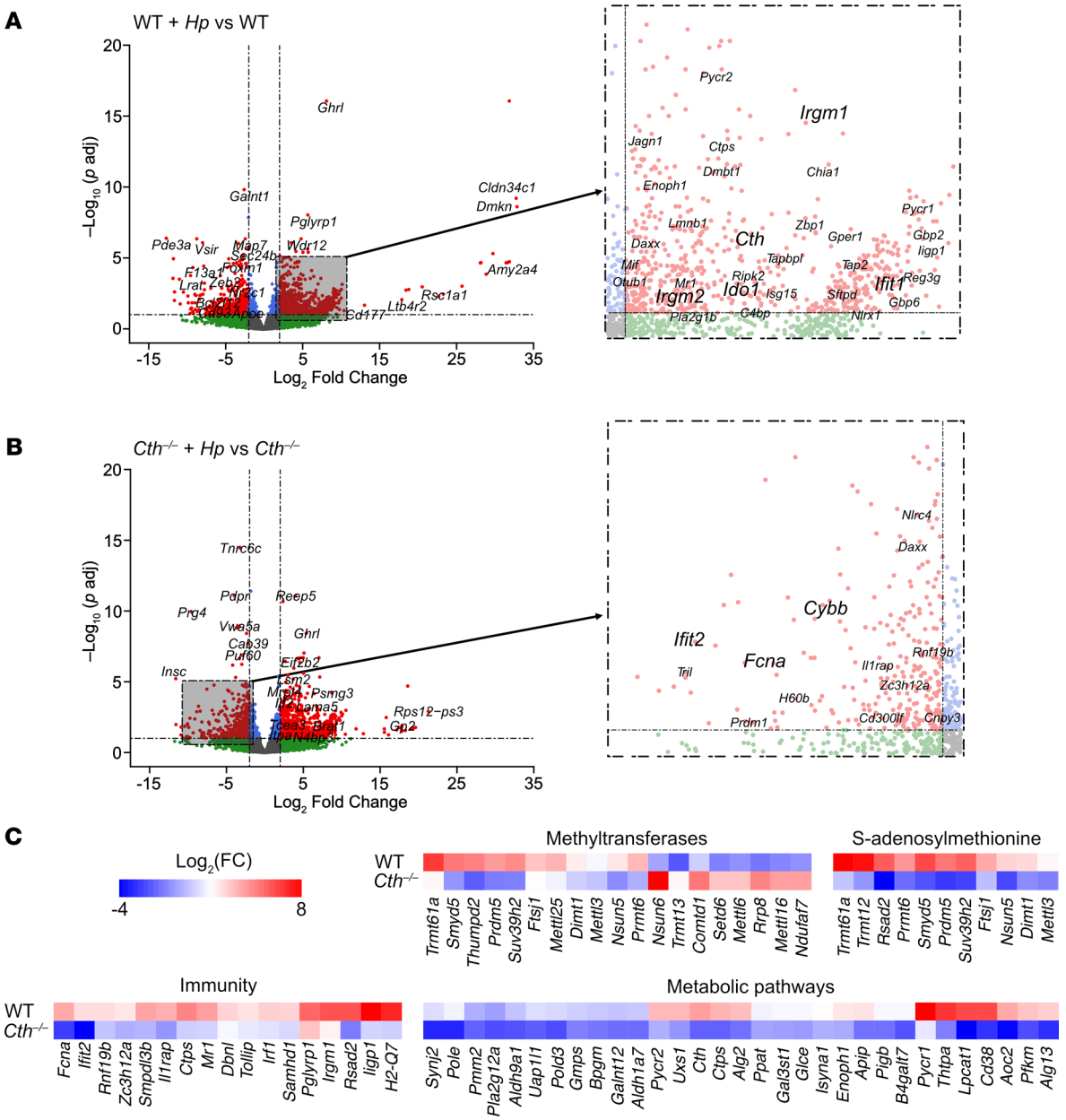

Figure 5. Identification of *H. pylori*–regulated genes in Gmacs. (**A** and **B**) The volcano plots show differential gene signatures in Gmacs from infected mice compared with uninfected mice (fold change [FC] > 2; FDR < 0.05). Gray dots, not significant; green dots, $\log_2$ fold change > 2; blue dots, adjusted (adj) $P < 0.05$; red dots, $\log_2$ fold change > 2 and adjusted $P < 0.05$. Genes of interest are enlarged. (**A**) Gmacs from *H. pylori*–infected WT mice compared with uninfected WT mice. (**B**) Gmacs from *H. pylori*–infected *Cth*$^{-/-}$ mice compared with uninfected *Cth*$^{-/-}$ mice. (**C**) Heatmaps displaying significantly altered pathways of DEGs in *Cth*$^{-/-}$ Gmacs compared with WT Gmacs of infected mice when compared with uninfected controls (interaction $P < 0.01$). Fold change is infected divided by control for each genotype.

We found that there were no significant differences in putrescine, spermidine, or spermine levels between WT and *Cth*$^{-/-}$ mice (Supplemental Figure 8A). This may be explained by the absence of any changes in the mRNA expression levels of enzymes within the polyamine pathway in the gastric tissues (Supplemental Figure 8B). We next directed the consumption of SAM toward the RTP and away from polyamine synthesis using the SAMDC inhibitor, SAM486A (also known as CGP 48664 and commercially as Sardomozide) (38). Inhibition of SAMDC in BMmacs resulted in a significant accumulation of putrescine with and without *H. pylori* infection (Supplemental Figure 8C). Spermidine levels remained relatively the same independent of treatment or infection, whereas spermine levels significantly decreased in *H. pylori*–infected cells after SAMDC inhibition (Supplemental Figure 8C). BMmacs treated with

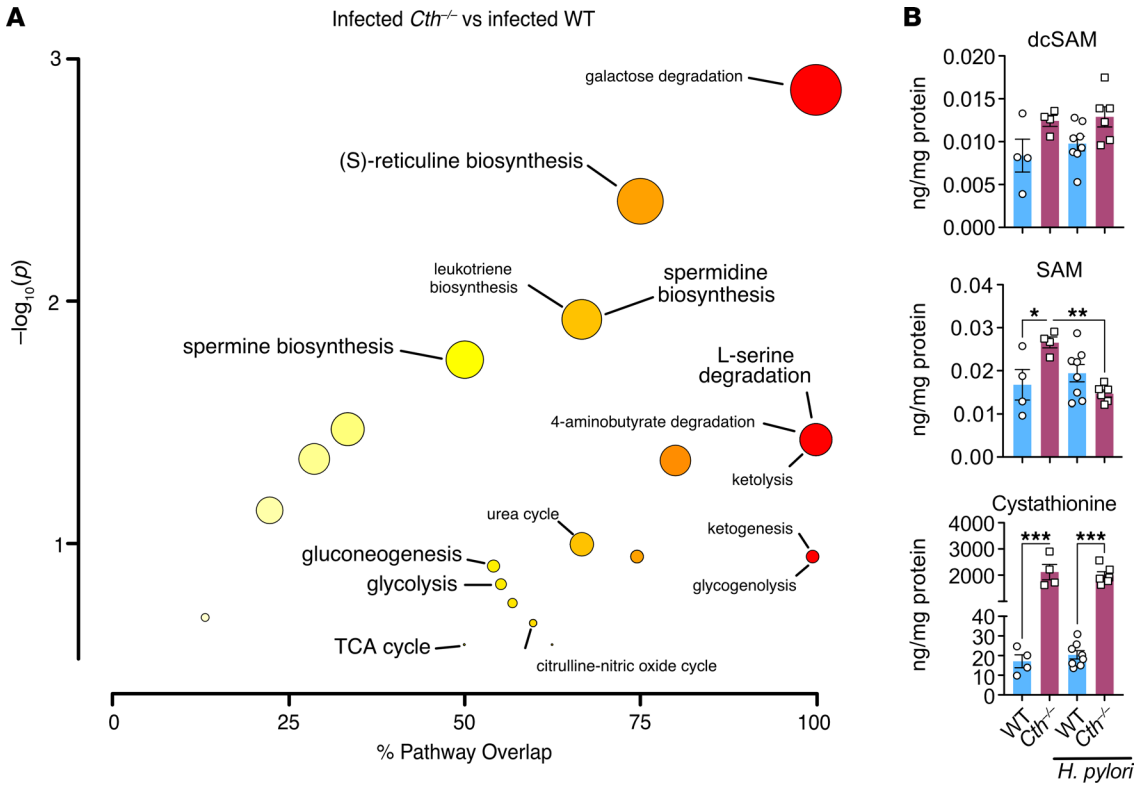

Figure 6. CTH promotes the metabolism of SAM through the RTP during *H. pylori* infection. (**A**) Bubble plot of metabolomic analysis of gastric tissues from WT and *Cth*$^{-/-}$ mice at 8 weeks p.i. with *H. pylori* PMSS1 (FDR < 0.05). Pathways involving SAM metabolism or energy production are enlarged. The *x*-axis and node color represent pathway overlap and the *y*-axis and node radius represent the *P* value; *n* = 8 infected mice per genotype. (**B**) Abundance of dcSAM, SAM, and cystathionine in the gastric tissues of WT and *Cth*$^{-/-}$ mice at 4 weeks p.i. with *H. pylori* PMSS1; *n* = 4 uninfected and 6–8 infected mice per genotype. All values are reported as mean ± SEM. Statistical analyses, where shown were conducted with 1-way ANOVA with Newman-Keuls post hoc test. **P* < 0.05, ***P* < 0.01, ****P* < 0.001.

SAM486A and infected with *H. pylori* for 24 hours displayed significantly increased expression of *Tnf* but decreased expression of *Il12b* compared with the untreated infected BMmacs (Supplemental Figure 8D). To assess the in vivo effect of SAMDC inhibition on *H. pylori*–induced disease, C57BL/6 mice were administered SAM486A by i.p. injection, beginning 1 week p.i., every other day for the remainder of the 4 week infection (Supplemental Figure 8E) (39). As expected, SAM486A treatment led to an increase of putrescine levels in the gastric tissues from the mice (Supplemental Figure 8F). In contrast, the levels of spermidine and spermine did not change with either infection or treatment with SAM486A (Supplemental Figure 8F), suggesting another mechanism maintains polyamine levels in the stomach. Mice treated with SAM486A had no change in gastritis scores or *H. pylori* colonization (Supplemental Figure 8, G and H). In summary, SAM supplementation and SAMDC inhibition had moderate effects on macrophage gene expression in vitro; however, this did not translate to in vivo effects, suggesting that SAM, SAMDC, and polyamines do not mediate the effects of CTH on *H. pylori*–induced inflammation and that other mechanisms should be identified.

CTH suppresses DNA methylation and supports activated macrophage gene expression. We observed that expression of CTH was specifically induced by *H. pylori* in BMmacs compared with another Gram-negative bacterium, *Citrobacter rodentium*, or the classical stimuli of M1-like macrophages (e.g., LPS plus IFN-γ), M2-like macrophages (e.g., IL-4), or regulatory macrophage–like macrophages (e.g., IL-10) (Figure 7A).

Currently available inhibitors of CTH are moderately selective but are active against other pyridoxal phosphate–dependent enzymes (40). Therefore, to assess the role of CTH in macrophages, we generated BMmacs from WT and *Cth*$^{-/-}$ mice (Figure 7B and Supplemental Figure 9A). We confirmed that CTH was not expressed in *Cth*$^{-/-}$ BMmacs (Supplemental Figure 9B) and that there was no change in expression of *Cbs* in the absence of CTH or after *H. pylori* infection (Supplemental Figure 9C). Levels of homocysteine, the substrate for transsulfuration, were significantly higher in *Cth*$^{-/-}$ BMmacs independent of infection, and

cystathionine levels were the same between WT and *Cth*$^{-/-}$ BMmacs with or without infection (Figure 7C and Supplemental Figure 9D). SAM levels were significantly higher in WT infected BMmacs compared with the uninfected control, whereas SAM levels were significantly decreased in *Cth*$^{-/-}$ BMmacs with and without *H. pylori* infection (Figure 7C and Supplemental Figure 9D). DNA methylation was significantly increased in infected *Cth*$^{-/-}$ BMmacs 6 hours p.i. with *H. pylori* (Figure 7, D and E). At 24 hours p.i., DNA methylation was reduced to almost uninfected WT levels; however, *Cth*$^{-/-}$ BMmacs had significantly higher levels of DNA methylation compared with WT, independent of infection (Supplemental Figure 9, E and F).

We next assessed whether the increase in DNA methylation affected gene expression. Levels of proinflammatory macrophage markers *Tnf*, *Nos2*, *Cxcl10*, *Il1b, Il6, and Il12b* were significantly reduced in *Cth*$^{-/-}$ BMmacs 6 hours p.i. with *H. pylori* (Figure 7F). The decreased *Nos2* mRNA expression in infected *Cth*$^{-/-}$ BMmacs correlated with decreased levels of NOS2 protein and NO production (Figure 7, G and H). Expression of the antiinflammatory markers *Chil3* and *Tgfb1*, but not *Arg1* and *Il10*, was decreased in *Cth*$^{-/-}$ BMmacs at 6 hours p.i. with *H. pylori* (Figure 7I). At 24 hours p.i. with *H. pylori*, expression of *Tnf*, *Arg1*, and *Tgfb1* was significantly reduced in *Cth*$^{-/-}$ BMmacs (Supplemental Figure 9, G and H). These findings support the idea that CTH can regulate macrophage gene expression through DNA methylation.

We have previously shown that *H. pylori* enhances macrophage gene expression through NF-κB activation (11, 41). We next found that WT and *Cth*$^{-/-}$ BMmacs had similar levels of MyD88 expression (Figure 7J), which is directly linked to TLR signaling upstream of NF-κB activation. In contrast, phosphorylation of the NF-κB p65 subunit RELA at Ser-536 that was activated by *H. pylori* infection in WT BMmacs was significantly decreased in *Cth*$^{-/-}$ cells (Figure 7J). NF-κB activation and nuclear translocation are regulated by the phosphorylation of inhibitor of κ light polypeptide gene enhancer in B cells, inhibitor α (NFKBIA, also known as IκBα), and subsequent degradation. There was no difference in the phosphorylation or total levels of NFKBIA (Supplemental Figure 9I). These findings suggest that CTH is important in early signaling cascades in macrophages by enhancing the phosphorylation of NF-κB, independent of NFKBIA degradation.

The role of CTH in the macrophage proteome. To further determine the role of CTH in the macrophage response to *H. pylori*, we analyzed the proteome of WT and *Cth*$^{-/-}$ BMmacs. Using a 4-plex tandem mass tag isobaric mass tagging–based approach, we identified 213 proteins in WT BMmacs and 142 proteins in *Cth*$^{-/-}$ BMmacs that were upregulated with infection, with 101 of those proteins shared between the 2 genotypes (Figure 8A and Supplemental Data Set 5). In addition, we identified 75 proteins in WT BMmacs and 45 proteins in *Cth*$^{-/-}$ BMmacs that were downregulated with infection, with 29 of those proteins shared between the 2 genotypes (Figure 8A and Supplemental Data Set 5). We then assessed the *H. pylori*–induced proteome of WT BMmacs using Ingenuity Pathway Analysis (Figure 8B and Supplemental Data Set 6). The pathway most significantly activated by infection was "metabolism of reactive oxygen species,"with a *Z*-score of 3.51 (Figure 8B and Supplemental Data Set 6).

We next assessed alterations in the *H. pylori*–induced proteome in the absence of CTH. *Cth*$^{-/-}$ BMmacs infected with *H. pylori* compared with uninfected *Cth*$^{-/-}$ BMmacs exhibited upregulation of only 27 of the 89 pathways (30%) activated by *H. pylori* infection in WT BMmacs (Figure 8C and Supplemental Data Set 7) and downregulation of only 2 of the 8 pathways (25%) inhibited by *H. pylori* infection in WT BMmacs (Supplemental Figure 10 and Supplemental Data Sets 6 and 7). Although "synthesis of reactive oxygen species" and "production of reactive oxygen species" were present in both WT and *Cth*$^{-/-}$ BMmacs, importantly, the "metabolism of reactive oxygen species" was not present in the pathways induced by *H. pylori* in *Cth*$^{-/-}$ BMmacs (Figure 8, B and C). Thus, CTH has the capacity to regulate protein expression in macrophages and contribute to macrophage activation and functions.

CTH supports mitochondrial respiration while promoting glycolysis in H. pylori–infected macrophages. To elucidate the mechanism by which CTH supports macrophage activation and contributes to *H. pylori*–induced disease, we investigated the downstream metabolic effects of *Cth* deletion in macrophages. Because the metabolomic pathway analysis indicated changes in glycolysis and the TCA cycle, we conducted extracellular flux assays on WT and *Cth*$^{-/-}$ BMmacs to assess mitochondrial function and cellular respiration. As expected, glycolysis and glycolytic capacity were increased with *H. pylori* infection in WT BMmacs, whereas *Cth*$^{-/-}$ BMmacs had impaired glycolysis and glycolytic capacity in naive cells or those exposed to *H. pylori* (Figure 9A). WT BMmacs stimulated with LPS plus IFN-γ for 24 hours had decreased oxygen consumption rate (OCR) but increased extracellular acidification rate (ECAR) (Supplemental Figure 11, A and B), whereas WT BMmacs stimulated with IL-4 for 24 hours displayed both increased OCR and increased ECAR (Supplemental Figure 11, C and D). Mitochondrial oxidative

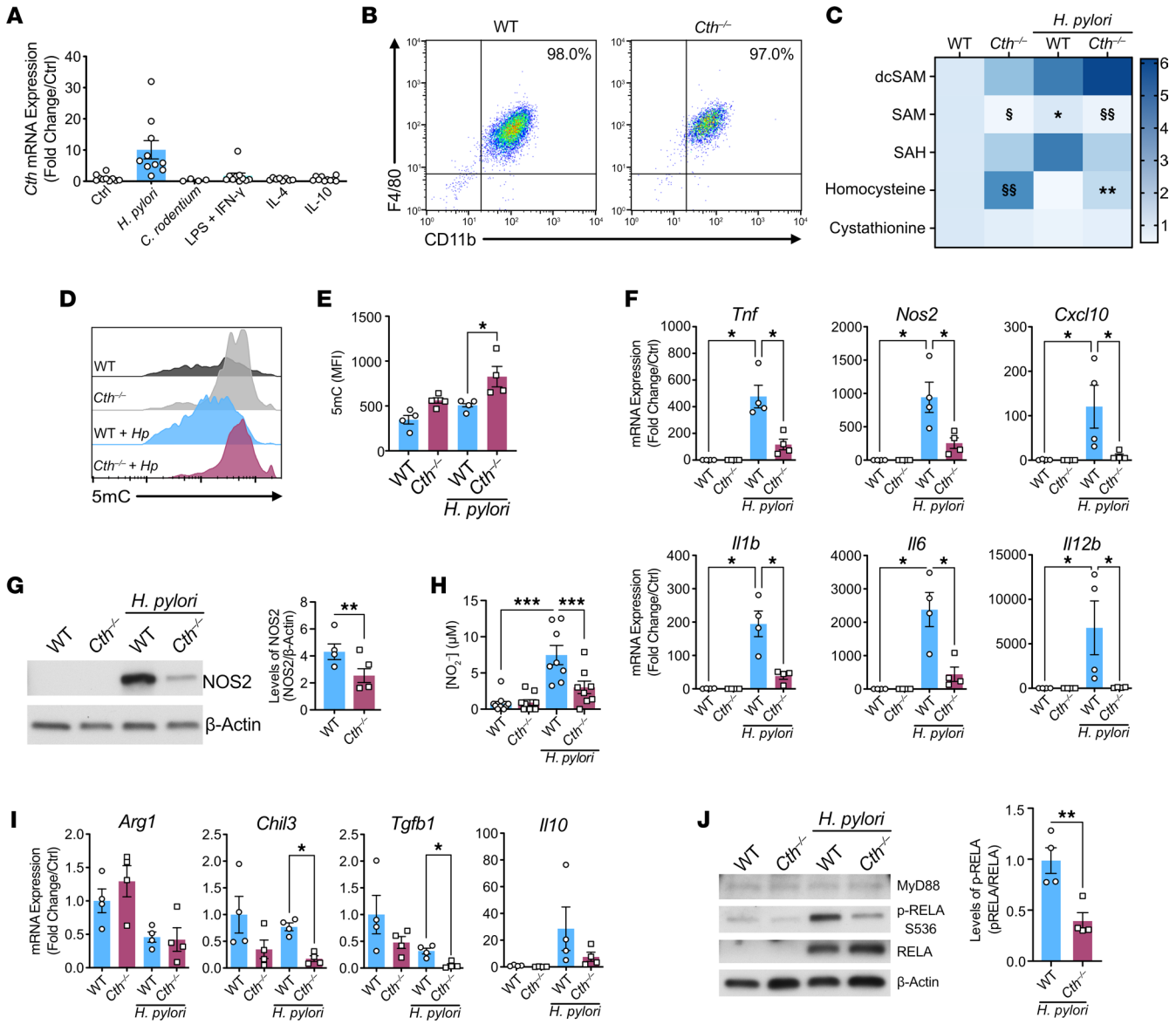

Figure 7. CTH suppresses DNA methylation and supports M1 macrophage gene expression. (**A**) Expression of *Cth* by WT BMmacs 24 hours after challenge; n = 4–10 biological replicates from 3 independent experiments. (**B**) Representative plot of CD11b and F4/80 expression of WT and *Cth*$^{-/-}$ BMmacs 24 hours p.i. with *H. pylori*. (**C**) Fold change of metabolite levels in BMmacs 24 hours p.i. with *H. pylori* compared with control (ctrl); n = 4 biological replicates. (**D**) Representative plot and (**E**) MFI quantification of 5mC staining in WT and *Cth*$^{-/-}$ BMmacs 6 hours p.i. with *H. pylori*; n = 4 biological replicates. (**F**) Expression of proinflammatory macrophage activation markers by WT and *Cth*$^{-/-}$ BMmacs 6 hours p.i. with *H. pylori*; n = 4–10 biological replicates per genotype from 3 independent experiments. (**G**) NOS2 protein immunoblot and densitometric analysis of WT and *Cth*$^{-/-}$ BMmacs 24 hours p.i. with *H. pylori*; n = 4 biological replicates per genotype. (**H**) NO_2^- concentration in supernatants from WT and *Cth*$^{-/-}$ BMmacs; n = 8 biological replicates from 2 independent experiments. (**I**) Expression of antiinflammatory macrophage activation markers by WT and *Cth*$^{-/-}$ BMmacs 6 hours p.i. with *H. pylori*; n = 4–10 biological replicates per genotype from 3 independent experiments. (**J**) Phosphorylated RELA (pRELA) protein immunoblot and densitometric analysis of WT and *Cth*$^{-/-}$ BMmacs 30 minutes p.i. with *H. pylori*; n = 3–4 biological replicates from 2 independent experiments. All values are reported as mean ± SEM. Statistical analyses, where shown: (**A**) 1-way ANOVA with Dunnett's test; (**C**) 1-way ANOVA with Newman-Keuls post hoc test; (**E**, **F**, **H**, and **I**) 1-way ANOVA with Kruskal-Wallis test, followed by a Mann-Whitney U test; (**J**) Student's t test. *P < 0.05, **P < 0.01, ***P < 0.001 vs. uninfected; §§P < 0.01 vs. WT.

phosphorylation was decreased (Figure 9B) and ECAR was increased with *H. pylori* infection in WT BMmacs (Figure 9C). *Cth*$^{-/-}$ BMmacs displayed increased OCR and ECAR 24 hours after challenge with *H. pylori* (Figure 9, B and C) or with LPS plus IFN-γ (Supplemental Figure 11, A and B) but did not change with IL-4 stimulation (Supplemental Figure 11, C and D). Uninfected *Cth*$^{-/-}$ BMmacs exhibited lower basal and maximal respiration than did uninfected WT BMmacs, which did not change with infection, unlike the WT BMmacs (Figure 9D). Elevated ECAR levels with *H. pylori* infection or LPS plus IFN-γ stimulation confirmed that the *Cth*$^{-/-}$ BMmacs were still viable (Figure 9C and Supplemental Figure 11B).

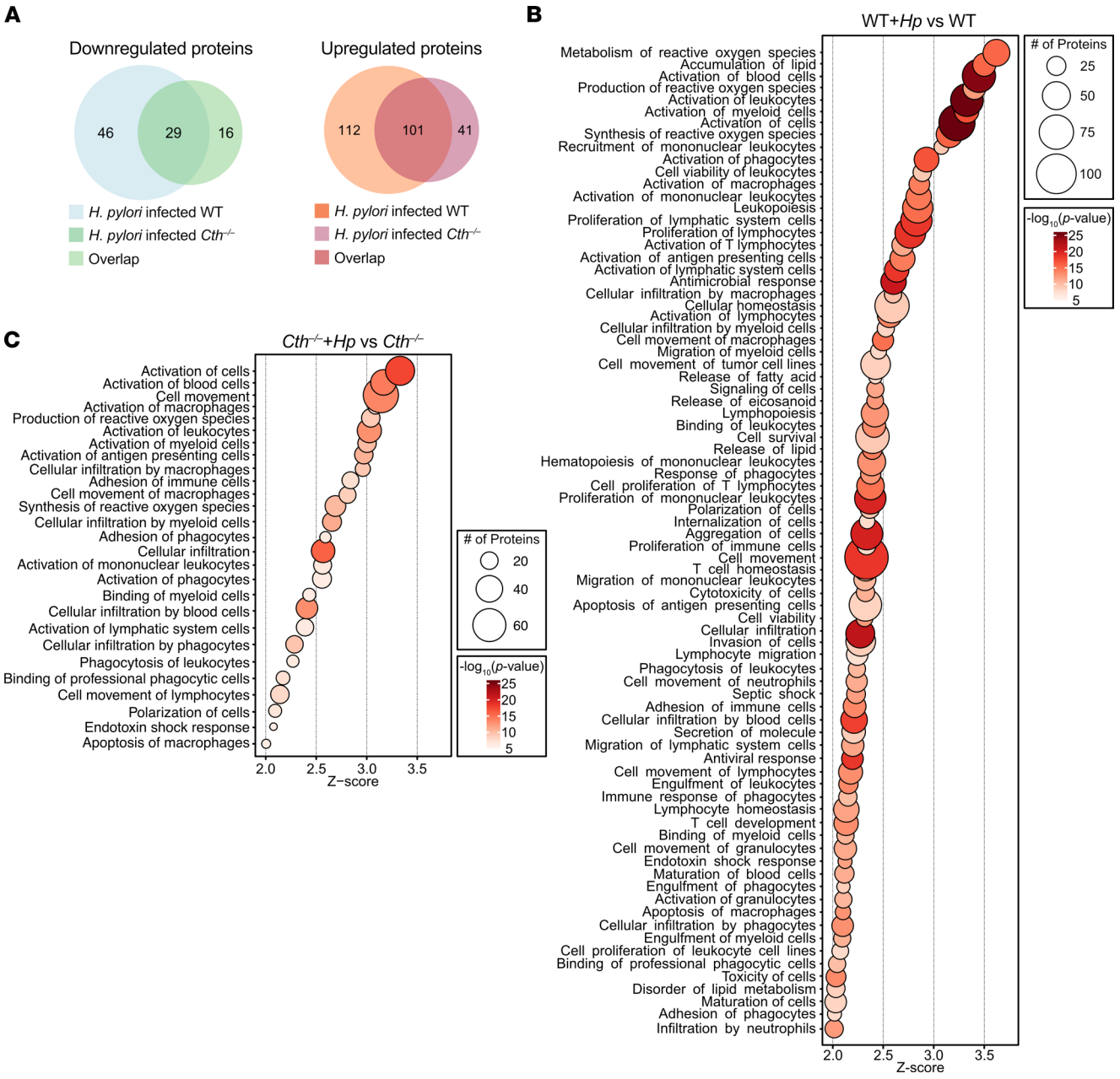

Figure 8. CTH modifies macrophage activation patterns of proteins during *H. pylori* infection. Proteomic analysis of BMmacs from WT and *Cth*$^{-/-}$ mice infected or not with *H. pylori* for 24 hours; $n = 4$ biological replicates per genotype. (**A**) Venn diagram showing commonly downregulated and upregulated proteins. (**B**) Enrichment analysis of pathways activated by *H. pylori* infection in WT BMmacs. (**C**) Enrichment analysis of the pathways in **B** activated by *H. pylori* infection in *Cth*$^{-/-}$ BMmacs. (FDR < 0.05; *Z*-score > 2).

The decreased mitochondrial respiration also resulted in decreased mitochondrial ATP production and spare respiratory capacity, an indicator of metabolic plasticity, in the *Cth*$^{-/-}$ BMmacs (Figure 9D), suggesting that *Cth*$^{-/-}$ BMmacs do not exhibit metabolic activation in response to infection.

Because mitochondrial activity contributes to the production of ROS that macrophages generate to combat pathogens, we measured mitochondrial superoxide levels, an indicator of mitochondrial ROS. We found that *H. pylori*–infected *Cth*$^{-/-}$ BMmacs exhibited a significant accumulation of mitochondrial ROS compared with uninfected controls and infected WT cells at 24 hours p.i. (Figure 9, E and F). We next measured the amount of the intracellular antioxidant glutathione (GSH) and found that GSH levels were low in *Cth*$^{-/-}$ BMmacs at baseline and remained unchanged with infection, whereas GSH levels decreased with infection in WT BMmacs (Figure 9G). Cysteine, the direct product of CTH activity, is a semi-essential

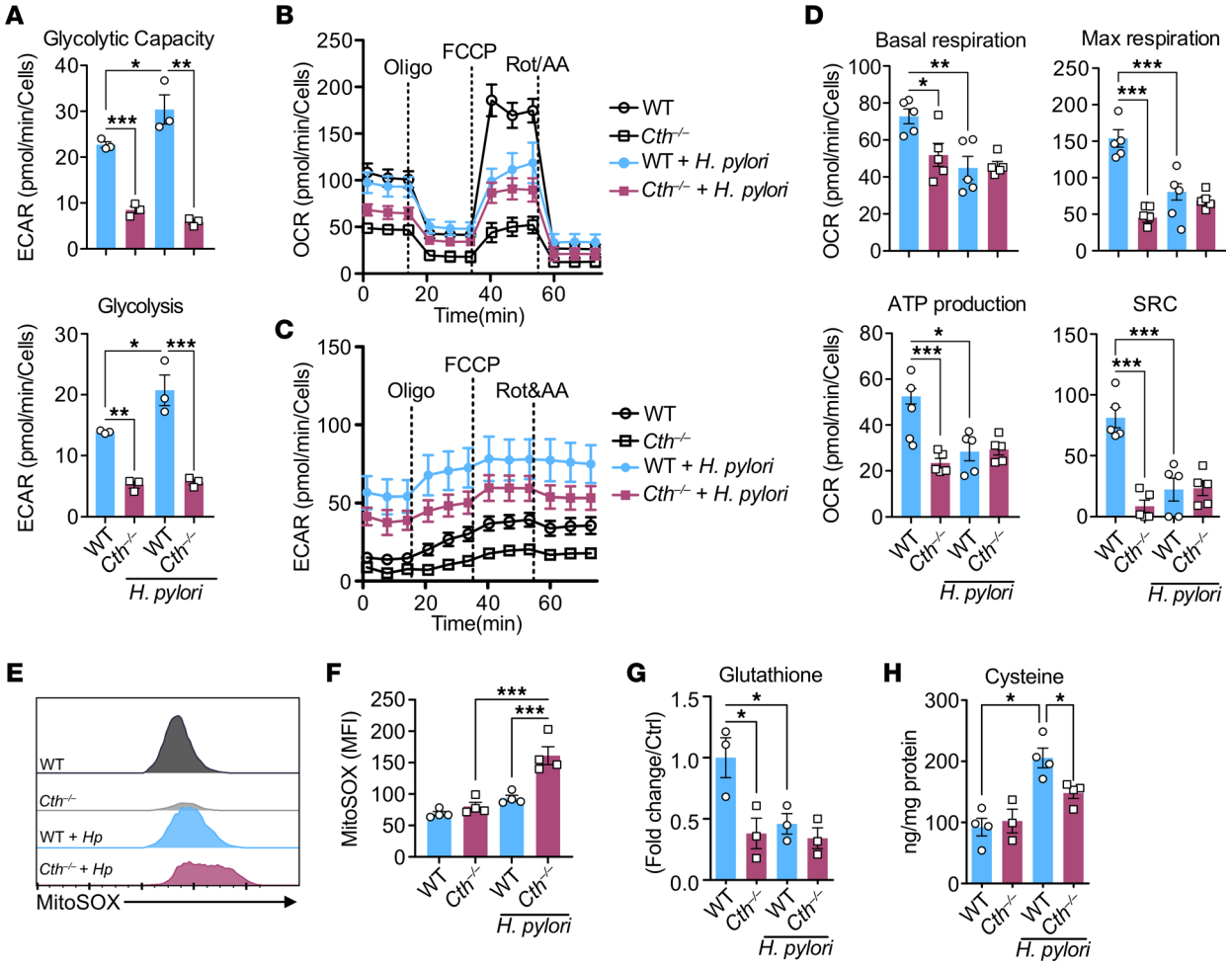

Figure 9. CTH contributes to macrophage activation by enhancing mitochondrial function and glycolysis in *H. pylori*–infected macrophages. (**A**) Rate of glycolysis and glycolytic capacity of WT and *Cth*$^{-/-}$ BMmacs 24 hours p.i. with *H. pylori*; *n* = 3 mice per genotype. (**B**) OCR and (**C**) ECAR of WT and *Cth*$^{-/-}$ BMmacs 24 hours p.i. with *H. pylori*; *n* = 5 from 2 independent experiments. Vertical dashed lines indicate the sequential addition of oligomycin (oligo), FCCP, and Rot/AA. (**D**) Basal respiration, maximal respiration, ATP production, and spare respiratory capacity (SRC) derived from **B**. (**E**) Representative plot and (**F**) MFI quantification of MitoSOX Red staining in WT and *Cth*$^{-/-}$ BMmacs 24 hours p.i. with *H. pylori*; *n* = 4 biological replicates. (**G**) Glutathione levels in WT and *Cth*$^{-/-}$ BMmacs 24 hours p.i. with *H. pylori*; n = 3 biological replicates. (**H**) Cysteine levels in WT and *Cth*$^{-/-}$ BMmacs 24 hours p.i. with *H. pylori*; *n* = 4 biological replicates. All values are reported as mean ± SEM. Statistical analyses, where shown: 1-way ANOVA with Newman-Keuls post hoc test. **P* < 0.05, ***P* < 0.01, ****P* < 0.001. FCCP, carbonyl cyanide-4 (trifluoromethoxy) phenylhydrazone; Max, maximum; Rot/AA (also Rot&AA), rotenone and antimycin A.

amino acid that is the main precursor for generation of GSH (15, 16). Cysteine levels were significantly elevated in infected WT BMmacs compared with control and infected *Cth*$^{-/-}$ BMmacs (Figure 9H), consistent with loss of CTH activity in *Cth*$^{-/-}$ BMmacs, and increased CTH activity with *H. pylori* infection in WT cells. These results suggest that macrophages upregulate CTH expression during *H. pylori* infection to maintain redox homeostasis.

Taken together, these studies demonstrate that the loss of CTH in macrophages leads to metabolic suppression and impaired immune activation that underlies the decrease in *H. pylori*–induced gastritis observed in *Cth*$^{-/-}$ mice (Supplemental Figure 12).

Discussion

Macrophages are a fundamental component of the host immune response with the capacity to transition along the spectrum of proinflammatory to antiinflammatory polarization as environmental signals and stimuli change (1, 2). In inflammatory pathologies, such as *H. pylori*–induced gastritis, overzealous immune responses can lead to more severe disease outcomes, such as gastric cancer (10). Therefore, identification of alternative strategies that target the host to limit chronic inflammatory conditions are

needed to prevent disease progression. Our study demonstrates that CTH affects metabolic activation and polarization of macrophages in response to *H. pylori* infection. Moreover, we used unbiased "omics" approaches to probe the global effects of CTH in the host response to *H. pylori* and consistently found evidence of a heightened immune response and enhanced cellular respiration in the presence of CTH that contributes to *H. pylori*–induced disease.

In several previous studies, researchers have investigated the role of CTH in inflammation within the context of H_2S production; however, there is not a consensus and results often depend on exogenous versus endogenous enzymatic H_2S derivation, with the latter being much less understood (42, 43). This variation in findings highlights the need to further characterize the role of CTH in different models of inflammation. Using a genetic model of *Cth* deletion, here we have shown that $Cth^{-/-}$ mice have significantly attenuated gastritis in models of acute and chronic *H. pylori* infection. In this study, we did not measure H_2S, because many bacterial pathogens, including *H. pylori* (44), produce H_2S, and host cells maintain the ability to produce H_2S in the absence of CTH through CBS or 3-mercaptopyruvate sulfurtransferase activity (15). Instead, we measured homocysteine, cystathionine, and cysteine levels as direct measures of CTH activity. Our work further supports the idea that CTH is a modulator of immune cell function and we have identified, for the first time, to our knowledge, the role of CTH in the stomach in the context of *H. pylori* infection. In future studies, it would be interesting to examine the interplay between CTH and the gut microbiome.

Our previous findings demonstrated that exogenous overexpression of the human *CTH* gene in RAW 264.7 cells inhibited markers of macrophage activation (33). However, determining the effect of CTH inhibition on macrophage activation was not feasible in the prior study, because we found that *Cth* siRNA diminished the number of live *H. pylori* in infected cells, potentially limiting the macrophage response, and that the CTH inhibitor aminooxyacetic acid directly kills *H. pylori* (33). In addition, the CTH inhibitor has off-target activity (33, 40). In the present study, genetic KO of *Cth* led to decreased macrophage activation during *H. pylori* infection. Transcriptomic analysis of Gmacs revealed that multiple gene sets involved in immune function were downregulated with *Cth* deletion. This was also reflected in the proteome of macrophages from $Cth^{-/-}$ versus WT mice infected ex vivo with *H. pylori*.

Because CTH has been mainly studied as a producer of H_2S, there is a gap in knowledge about how CTH may influence the metabolic pathways directly upstream of its activity. Our analysis of untargeted metabolomics identified SAM metabolism and cellular respiration as pathways regulated by CTH. SAM supplementation has been shown to reduce airway inflammation (45), and M1-like macrophages exhibit reduced DNA methylation (46, 47). However, *S*-adenosylhomocysteine, the product of methyl donation by SAM, can bind to methyltransferases and inhibit methylation reactions (48, 49). Although SAM supplementation suppressed proinflammatory and enhanced antiinflammatory gene expression in vitro, there was no protection from *H. pylori* gastritis in vivo. The polyamine pathway is directly linked to SAM metabolism. Based on the increased gastritis in mice with myeloid-specific deletion of ornithine decarboxylase during *H. pylori* infection (12), we anticipated that inhibition of SAMDC would result in the accumulation of putrescine and decreased inflammation. However, we observed that SAMDC inhibition increased putrescine levels in the stomach of mice without affecting gastritis, suggesting that putrescine accumulation alone is not sufficient to regulate gastritis. Similarly, we hypothesized that deletion of CTH might free up SAM for the metabolism of putrescine into spermidine and increase inflammation. However, loss of CTH did not alter polyamine levels sufficiently enough to affect gastritis.

There is a growing body of literature describing the metabolic needs of immune cells and, in particular, the role of metabolism in macrophage differentiation and activation (50, 51). During macrophage stimulation, polarizing macrophages remodel their metabolism to meet energetic needs. Proinflammatory macrophages repress oxidative phosphorylation in favor of glycolysis to aid the production of cytokines and ROS (52). In contrast, antiinflammatory M2 macrophages enhance mitochondrial oxidative phosphorylation while still consuming glucose (53). We found that macrophages lacking CTH have impaired ability to metabolically adapt to external stimuli. ROS and nitrogen species are important effector molecules produced by macrophages to combat pathogens and regulate polarization (54); however, high levels can be detrimental and cause cellular dysfunction, including mitochondrial impairment (55). Consistent with these concepts, our findings show that loss of CTH results in depleted intracellular cysteine and GSH and contributes to high levels of mitochondrial superoxide and reduced mitochondrial function. Beyond the altered gene expression of macrophage cytokines, our data highlight an unexpected role of CTH in macrophage metabolism and respiration.

Last, in the context of *H. pylori* infection, regulation of TNF-α transcription depends on alternative activation of NF-κB through the phosphorylation of the p65 subunit RELA at Ser-536 that does not involve NFKBIA degradation (56). We found that deletion of *Cth* led to decreased TNF-α expression during infection with *H. pylori*, in vitro and in vivo, and with LPS plus IFN-γ stimulation. The impaired cytokine production may be linked to the observed decrease in phosphorylation of RELA at Ser-536 in the infected $Cth^{-/-}$ macrophages, especially because there were no differences in phospho- or total NFKBIA levels between the infected cells. Because many kinases are involved in the phosphorylation of p65, future studies using various receptor and signaling cascade inhibitors may enhance the understanding of the mechanism connecting CTH with the early macrophage responses.

In summary, our findings outline the role of CTH in regulating the macrophage-facilitated response to *H. pylori*. Increased expression of CTH by macrophages contributes to inflammation in the gastric tissues of mice and markers of proinflammatory macrophages ex vivo in the context of *H. pylori* infection. Using genetic deletion of *Cth*, we determined that CTH can affect macrophage function via enhanced gene and protein expression through NF-κB phosphorylation and suppression of DNA methylation and maintenance of mitochondrial function through redox homeostasis. These activities, in turn, can affect the adaptive immune response in T cells, though *Cth* deletion does not appear to affect T cell function in a cell-autonomous manner. Because of the limitations of current chemical inhibitors of CTH, exploring the full spectrum of pathways related to CTH is essential in the discovery of therapeutic targets that can help reduce the burden of chronic gastritis and risk of gastric cancer in humans.

Methods

See Supplemental Methods for detailed experimental procedures.

Materials and reagents. See Supplemental Table 1 for information regarding reagents and kits used in this study. See Supplemental Table 2 for information regarding software and analysis packages used in this study. See Supplemental Table 3 for information regarding Abs used in this study. See Supplemental Table 4 for information regarding RT-PCR primers used in this study

Statistics. All the data shown represent the mean ± SEM. A minimum of 3 biological replicates were used for in vitro studies. Statistical analysis was performed in GraphPad Prism 9.2 (GraphPad Software), and significance was set at $P < 0.05$. Where data were normally distributed, 2-tailed Student's *t* test and 1-way ANOVA with the Newman-Keuls or Dunnett's post hoc test were used to determine significant differences between 2 groups or multiple test groups, respectively. Where data were not normally distributed, a 1-way ANOVA with the Kruskal-Wallis test, followed by a Mann-Whitney *U* test, was performed, unless otherwise noted. Detailed statistical analysis for RNA-Seq, metabolomics, and proteomics are included in Supplemental Methods.

Study approval. Mice were used under the protocols M1900034, V1800106, and V2000018 approved by the IACUC at Vanderbilt University and Institutional Biosafety Committee and the Research and Development Committee of the Veterans Affairs Tennessee Valley Healthcare System. Procedures were performed in accordance with institutional policies, AAALAC guidelines, the American Veterinary Medical Association Guidelines on Euthanasia, NIH regulations (*Guide for the Care and Use of Laboratory Animals*; National Academies Press, 2011), and the US Animal Welfare Act (1966).

Author contributions

YLL, APG, and KTW conceived of the study; DPB contributed to methodology; YLL, APG, JLF, MA, KMM, TMS, DPB, MMA, AGD, MBP, PBL, CS, GLM, and JCS conducted the investigation; YLL and KLR conducted the formal analysis; JJ, JAG, BDP, and SHS provided resources; YLL, KLR, MWC, and KLS contributed to data curation; YLL contributed to visualization during the studies and wrote the original draft of the manuscript; YLL, APG, and KTW reviewed and edited the manuscript; APG and KTW supervised conducting of the study; and KTW acquired funding for the study.

Acknowledgments

This work was funded by NIH grants R21AI142042, R01CA190612, P01CA116087, P01CA028842, and R01DK128200 (to KTW); Veterans Affairs Merit Review grants I01BX001453 and I01CX002171 (to KTW); Department of Defense grant W81XWH-18-1-0301 (to KTW); Senior Research Award 703003 from the Crohn's & Colitis Foundation (to KTW); the Thomas F. Frist Sr. Endowment (to KTW); and the

Vanderbilt Center for Mucosal Inflammation and Cancer (to KTW). YLL was supported by NIH grant T32AI138932, and KMM was supported by NIH grant T32CA009592. JJ was supported by an Academy Ter Meulen Grant from the Royal Netherlands Academy of Arts and Sciences and a grant from the Prince Bernhard Cultural Foundation. Proteomics and metabolomics analyses were supported in part by Core Scholarships from the Vanderbilt University Medical Center Digestive Disease Research Center, funded by NIH grant P30DK058404, the Vanderbilt Ingram Cancer Center support grant P30CA068485, and NIH grant S10OD023514 (to KLS). Generation of *Cth*-deficient mice was supported by NIH grant P50DA044123 (to SHS) and the American Heart Association–Allen Initiative in Brain Health and Cognitive Impairment grant 19PABHI34580006 (to SHS and BDP).

Address correspondence to: Keith T. Wilson, Vanderbilt University Medical Center, 2215B Garland Ave., 1030C MRB IV, Nashville, Tennessee 37232-0252, USA. Phone: 615.343.5675; Email: keith.wilson@vumc.org.

1. Benoit M, et al. Macrophage polarization in bacterial infections. *J Immunol*. 2008;181(6):3733–3739.
2. Mosser DM, Edwards JP. Exploring the full spectrum of macrophage activation. *Nat Rev Immunol*. 2008;8(12):958–969.
3. Murray PJ, Wynn TA. Protective and pathogenic functions of macrophage subsets. *Nat Rev Immunol*. 2011;11(11):723–737.
4. Wilson KT, et al. Helicobacter pylori stimulates inducible nitric oxide synthase expression and activity in a murine macrophage cell line. *Gastroenterology*. 1996;111(6):1524–1533.
5. Gobert AP, et al. Helicobacter pylori arginase inhibits nitric oxide production by eukaryotic cells: a strategy for bacterial survival. *Proc Natl Acad Sci U S A*. 2001;98(24):13844–13849.
6. Chaturvedi R, et al. Polyamines impair immunity to Helicobacter pylori by inhibiting L-arginine uptake required for nitric oxide production. *Gastroenterology*. 2010;139(5):1686–1698.
7. Chaturvedi R, et al. Spermine oxidase mediates the gastric cancer risk associated with Helicobacter pylori CagA. *Gastroenterology*. 2011;141(5):1696–1708.
8. Lewis ND, et al. Arginase II restricts host defense to Helicobacter pylori by attenuating inducible nitric oxide synthase translation in macrophages. *J Immunol*. 2010;5(184):2572–2582.
9. Chaturvedi R, et al. Increased Helicobacter pylori-associated gastric cancer risk in the Andean region of Colombia is mediated by spermine oxidase. *Oncogene*. 2015;34(26):3429–3440.
10. Hardbower DM, et al. At the bench: Helicobacter pylori, dysregulated host responses, DNA damage, and gastric cancer. *J Leukoc Biol*. 2014;96(2):201–212.
11. Hardbower DM, et al. EGFR regulates macrophage activation and function in bacterial infection. *J Clin Invest*. 2016;9(126):3296–3312.
12. Hardbower DM, et al. Ornithine decarboxylase regulates M1 macrophage activation and mucosal inflammation via histone modifications. *Proc Natl Acad Sci U S A*. 2017;114(5):E751–E760.
13. Gobert AP, et al. Hypusination orchestrates the antimicrobial response of macrophages. *Cell Rep*. 2020;33(11):108510.
14. Shapouri-Moghaddam A, et al. Macrophage plasticity, polarization, and function in health and disease. *J Cell Physiol*. 2018;233(9):6425–6440.
15. Singh S, et al. Relative contributions of cystathionine beta-synthase and gamma-cystathionase to H2S biogenesis via alternative trans-sulfuration reactions. *J Biol Chem*. 2009;284(33):22457–22466.
16. Chiku T, et al. H2S biogenesis by human cystathionine gamma-lyase leads to the novel sulfur metabolites lanthionine and homolanthionine and is responsive to the grade of hyperhomocysteinemia. *J Biol Chem*. 2009;284(17):11601–11612.
17. Lio C-WJ, Huang SC-C. Circles of life: linking metabolic and epigenetic cycles to immunity. *Immunology*. 2020;161(3):165–174.
18. Pegg AE. Mammalian polyamine metabolism and function. *IUBMB Life*. 2009;61(9):880–894.
19. Hooi JKY, et al. Global prevalence of Helicobacter pylori infection: systematic review and meta-analysis. *Gastroenterology*. 2017;153(2):420–429.
20. Sung H, et al. Global Cancer Statistics 2020: GLOBOCAN estimates of incidence and mortality worldwide for 36 cancers in 185 countries. *CA Cancer J Clin*. 2021;71(3):209–249.
21. Parsonnet J, et al. Risk for gastric cancer in people with CagA positive or CagA negative Helicobacter pylori infection. *Gut*. 1997;40(3):297–301.
22. Plummer M, et al. Global burden of gastric cancer attributable to Helicobacter pylori. *Int J Cancer*. 2015;136(2):487–490.
23. Mannion A, et al. Helicobacter pylori antimicrobial resistance and gene variants in high- and low-gastric-cancer-risk populations. *J Clin Microbiol*. 2021;59(5):e03203–20.
24. Saracino IM, et al. Next generation sequencing for the prediction of the antibiotic resistance in Helicobacter pylori: a literature review. *Antibiotics (Basel)*. 2021;10(4):437.
25. Savoldi A, et al. Prevalence of antibiotic resistance in Helicobacter pylori: a systematic review and meta-analysis in World Health Organization regions. *Gastroenterology*. 2018;155(5):1372–1382.
26. Piazuelo MB, et al. The Colombian Chemoprevention Trial: 20-year follow-up of a cohort of patients with gastric precancerous lesions. *Gastroenterology*. 2021;160(4):1106–1117.
27. Mera RM, et al. Dynamics of Helicobacter pylori infection as a determinant of progression of gastric precancerous lesions: 16-year follow-up of an eradication trial. *Gut*. 2018;67(7):1239–1246.
28. Huang RJ, et al. A summary of the 2020 Gastric Cancer Summit at Stanford University. *Gastroenterology*. 2020;159(4):1221–1226.
29. Correa P. Human gastric carcinogenesis: a multistep and multifactorial process--First American Cancer Society Award Lecture on Cancer Epidemiology and Prevention. *Cancer Res*. 1992;52(24):6735–6740.

30. Peek RM, et al. Role of innate immunity in Helicobacter pylori-induced gastric malignancy. *Physiol Rev*. 2010;90(3):831–858.
31. Hardbower DM, et al. Chronic inflammation and oxidative stress: the smoking gun for Helicobacter pylori-induced gastric cancer? *Gut Microbes*. 2013;4(6):475–481.
32. Piazuelo MB, et al. Resolution of gastric cancer-promoting inflammation: a novel strategy for anti-cancer therapy. *Curr Top Microbiol Immunol*. 2019;421:319–359.
33. Gobert AP, et al. Bacterial pathogens hijack the innate immune response by activation of the reverse transsulfuration pathway. *mBio*. 2019;10(5):e02174–19.
34. Yang G, et al. H2S as a physiologic vasorelaxant: hypertension in mice with deletion of cystathionine gamma-lyase. *Science*. 2008;322(5901):587–590.
35. Sierra JC, et al. Epidermal growth factor receptor inhibition downregulates Helicobacter pylori-induced epithelial inflammatory responses, DNA damage and gastric carcinogenesis. *Gut*. 2018;67(7):1247–1260.
36. Lewis ND, et al. Immune evasion by Helicobacter pylori is mediated by induction of macrophage arginase II. *J Immunol*. 2011;186(6):3632–3641.
37. Sierra JC, et al. Spermine oxidase mediates Helicobacter pylori-induced gastric inflammation, DNA damage, and carcinogenic signaling. *Oncogene*. 2020;39(22):4465–4474.
38. Svensson F et al. CGP 48664, a potent and specific S-adenosylmethionine decarboxylase inhibitor: effects on regulation and stability of the enzyme. *Biochem J*. 1997;322(pt 1):297–302.
39. Zabala-Letona A, et al. MTORC1-dependent AMD1 regulation sustains polyamine metabolism in prostate cancer. *Nature*. 2017;547(7661):109–113.
40. Asimakopoulou A, et al. Selectivity of commonly used pharmacological inhibitors for cystathionine β synthase (CBS) and cystathionine γ lyase (CSE). *Br J Pharmacol*. 2013;169(4):922–932.
41. Asim M, et al. Helicobacter pylori induces ERK-dependent formation of a phospho-c-Fos c-Jun activator protein-1 complex that causes apoptosis in macrophages. *J Biol Chem*. 2010;285(26):20343–20357.
42. Dilek N, et al. Hydrogen sulfide: an endogenous regulator of the immune system. *Pharmacol Res*. 2020;161:105119.
43. Rahman MA, et al. Hydrogen sulfide dysregulates the immune response by suppressing central carbon metabolism to promote tuberculosis. *Proc Natl Acad Sci U S A*. 2020;117(12):6663–6674.
44. Lee H, et al. Volatile sulfur compounds produced by Helicobacter pylori. *J Clin Gastroenterol*. 2006;40(5):421–426.
45. Yoon S-Y, et al. S-adenosylmethionine reduces airway inflammation and fibrosis in a murine model of chronic severe asthma via suppression of oxidative stress. *Exp Mol Med*. 2016;48(6):e236.
46. Jain N, et al. Global modulation in DNA epigenetics during pro-inflammatory macrophage activation. *Epigenetics*. 2019;14(12):1183–1193.
47. Travers M, et al. DFMO and 5-azacytidine increase M1 macrophages in the tumor microenvironment of murine ovarian cancer. *Cancer Res*. 2019;79(13):3445–3454.
48. Hoffman DR, et al. Relationship between tissue levels of S-adenosylmethionine, S-adenosylhomocysteine, and transmethylation reactions. *Can J Biochem*. 1979;57(1):56–64.
49. Caudill MA, et al. Intracellular S-adenosylhomocysteine concentrations predict global DNA hypomethylation in tissues of methyl-deficient cystathionine beta-synthase heterozygous mice. *J Nutr*. 2001;131(11):2811–2818.
50. Langston PK, et al. Metabolism supports macrophage activation. *Front Immunol*. 2017;8:61.
51. Wang J, et al. MARRVEL: integration of human and model organism genetic resources to facilitate functional annotation of the human genome. *Am J Hum Genet*. 2017;100(6):843–853.
52. Freemerman AJ, et al. Metabolic reprogramming of macrophages: glucose transporter 1 (GLUT1)-mediated glucose metabolism drives a proinflammatory phenotype. *J Biol Chem*. 2014;289(11):7884–7896.
53. Huang SC-C, et al. Metabolic reprogramming mediated by the mTORC2-IRF4 signaling axis is essential for macrophage alternative activation. *Immunity*. 2016;45(4):817–830.
54. Tan H-Y, et al. The reactive oxygen species in macrophage polarization: reflecting its dual role in progression and treatment of human diseases. *Oxid Med Cell Longev*. 2016;2016:2795090.
55. Wang P, et al. Macrophage achieves self-protection against oxidative stress-induced ageing through the Mst-Nrf2 axis. *Nat Commun*. 2019;10(1):755.
56. Ahmed AU, et al. Integrin-linked kinase modulates lipopolysaccharide- and Helicobacter pylori-induced nuclear factor κB-activated tumor necrosis factor-α production via regulation of p65 serine 536 phosphorylation. *J Biol Chem*. 2014;289(40):27776–27793.